Sediment recycling by continental subduction indicated by B-Hf-Pb-Nd isotopes from Miocene–Quaternary lavas in the northern margin of Tibet

Xiu-Zheng Zhang [a, b], Qiang Wang[a, b, c*], Andrew C. Kerr[d], Gang-Jian Wei[a, b], Yue Qi[a], Ying Liu[a], Yu-Cheng Yang[a]

[a] *State Key Laboratory of Isotope Geochemistry, Guangzhou Institute of Geochemistry, Chinese Academy of Sciences, Guangzhou 510640, China*

[b] *CAS Center for Excellence in Deep Earth Science, Guangzhou, 510640, China*

[c] *College of Earth and Planetary Sciences, University of Chinese Academy of Sciences, Beijing 100049, China*

[d] *School of Earth and Environmental Sciences, Cardiff University, Cardiff CF10 3AT, UK*

Corresponding Author:

* Qiang Wang, State Key Laboratory of Isotope Geochemistry (SKLaBIG), Guangzhou Institute of Geochemistry (GIG), Chinese Academy of Sciences (CAS), Wushan Street, Guangzhou, 510640, Tel: +8615724063366, Fax: 86-20-85290130; E-mail: wqiang@gig.ac.cn

Abstract

Although it has been argued that sediment recycling plays an important role in the differentiation of the continental crust, boron (B) isotopic data does not support a direct input of subducted sediments into arc magmas. This raises questions about the viability of sediment recycling as a process in the differentiation of continental crust. Here, we report B isotopic data from Miocene–Quaternary lavas derived from different sources in the northern margin of Tibet. These lavas have high B contents and negative $\delta^{11}B$ values close to those of continental sediments. Strongly peraluminous rhyolites have the highest B (93 to 1559 ppm) contents with negative $\delta^{11}B$ (−9.7 to −17.9) values. Adakitic dacites and trachyandesites exhibit the lowest B (18 to 29 ppm) contents with markedly negative $\delta^{11}B$ (−12.0 to −35.7) values whereas olivine leucitites have B (37.2 to 59.3 ppm) contents with negative $\delta^{11}B$ (−8.3 to −15.6) values. These lavas also have enriched Hf-Pb-Nd isotopic compositions similar to those of sediments. This data, combined with numerical modelling and geophysical and tectonic data for Cenozoic continental subduction in the northern margin of Tibet, indicates that: (1) the strongly peraluminous rhyolites were generated by partial melting of mica-bearing continental sedimentary rocks subducted to the depth of mid-to-lower crust; (2) adakitic lavas were derived by partial melting of sediment-bearing thickened lower crust underwent dehydration and eclogites-facies metamorphism; and (3) olivine leucitites were generated by partial melting of enriched mantle metasomatized by sediment-bearing eclogite-facies crust-derived melts. Thus, at continental convergent margins, continental subduction is an important mechanism for sediment recycling and the evolution of continental crust.

Keywords:

Boron isotopes; Continental subduction; Sediment recycling; Miocene–Quaternary; Tibetan Plateau

Highlights:

- B-Hf-Pb-Nd isotopes reveal that subducted continental sediments entered the mid-to-lower crust and mantle of northern Tibet.
- Subducted sediments in mid-to-lower crust and mantle were recycled to the continental crust via magmatism.
- Continental subduction is an important mechanism for sediment recycling and the evolution of continental crust.

1. Introduction

The continental crust has an andesitic bulk composition, this is however inconsistent, with the predominantly basaltic magmas that contribute to the present-day continental crust (Rudnick, 1995; Hawkesworth and Kemp, 2006). To solve this discrepancy, a range of models for the differentiation of the continental crust have been proposed, including the removal of Mg through chemical weathering (Lee et al., 2008; Shen et al., 2009; Liu and Rudnick, 2011), direct addition of intermediate-acid magmas to the crust through melting of subducted oceanic slab (Defant and Drummond, 1990; Gazel et al., 2015) or basaltic lower crust (Atherton and Petford, 1993), removal of mafic/ultramafic lower crust through foundering/delamination (Arndt and Goldstein, 1989; Kay and Kay, 1993; Rudnick, 1995; Jull and Kelemen, 2001), the reworking of sedimentary materials by mantle-like magmas (Kemp et al., 2007), or subduction of continental or oceanic crust followed by "relamination" of buoyant and felsic crust (Hacker et al., 2011).

It is clear, however, that the recycling of crustal materials plays an important role in the differentiation of continental crust. Moreover, some crustal materials may also be recycled into mantle, thereby contributing to mantle heterogeneity (Plank and Langmuir, 1993; Liu and Rudnick, 2011). For example, in island arc zones, sediments from subducted oceanic slabs have been suggested to recycle to the continental crust through arc magmatism (Plank and Langmuir, 1993; Hawkesworth et al., 1997; Behn et al., 2011; Marschall and Schumacher, 2012) or relamination (Hacker et al., 2011), or directly enter the overlying mantle wedge by the buoyant diapir rise due to their low density (Behn et al., 2011; Marschall and Schumacher, 2012).

Boron is an excellent tracer of crustal recycling at convergent margins, given its high concentration in subducted sediments and altered oceanic crust (AOC) relative to mantle or mantle-derived fresh rocks. Furthermore, it is highly mobile during partial melting and dehydration, and its isotopes are strongly fractionated during their transfer in seawater or crust (Morris et al., 1990; Palmer, 1991; Moran et al., 1992; Edwards et al., 1993; Ishikawa and Nakamura, 1994; Chaussidon and Marty, 1995; Leeman and Sisson, 1996). In addition, several studies have demonstrated substantial differences in the $\delta^{11}B$ values of subducted continental sediments, marine sediments, and AOC (Ishikawa and Nakamura, 1994; Chaussidon and Marty, 1995; Leeman and Sisson, 1996; Rose et al., 2001; Clift et al., 2003; Yamaok et al., 2012), highlighting the unparalleled advantage of B isotopes in tracing recycling processes in subduction zones (Palmer, 2017; De Hoog and Savov, 2018; Wang et al., 2020).

Nd-Hf-Pb isotopic systematics reveal that sediments from subducted oceanic slabs are recycled to the continental crust by arc magmatism (Plank and Langmuir, 1993; Hawkesworth et al., 1997; Shimoda et al., 1998; Chauvel et al., 2008; Behn et al., 2011; Marschall and Schumacher, 2012). However, paradoxically, B isotopic data suggests that arc magmatic rocks are derived from mantle wedge metasomatized by fluids released from subducted basaltic oceanic crust and overlying sediments, rather than directly from subducted sediments themselves (Morris et al., 1990; Edwards et al., 1993; Ishikawa and Nakamura, 1994; Leeman and Sisson, 1996; Smith et al., 1997; Clift et al., 2003). In other words, many arc lavas contain material derived from subducted oceanic crust and sediments, but it remains unresolved whether this distinctive geochemical signature is transferred from the subducting slab by aqueous fluids, oceanic crust or sediment-derived silicate melts, or both (Peacock and Hervig, 1999). It therefore remains unclear whether subducted sediments can reenter the continental crust via arc magmatism. This raises questions about the possibility of sediment recycling in the differentiation of continental crust.

Unlike island arcs, the Cenozoic Himalayan-Tibetan Orogen resulted from the convergence (collision or continental subduction) processes between the Indian and Eurasian continents (Yin and Harrison, 2000; Chung et al., 2005). Apart of this process the Indian and Eurasian continents are subducting northward and southward beneath the Tibetan lithosphere, respectively (Kind et al., 2002; McKenzie and Priestley, 2008; Nábelek et al., 2009; Zhao et al., 2010, 2011; Ma et al., 2021; Hao et al., 2022). As a result Cenozoic magmatic rocks widely occur in Himalayan-Tibetan Orogen, and were derived by partial melting of mid-to-lower crustal sedimentary rocks (e.g., Himalayan leucogranites and northern Tibet tourmaline-bearing mica rhyolites) (e.g., Patiño Douce and Harris, 1998; Knesel and Davidson, 2002; Guo and Wilson, 2012; Wang et al., 2012), thickened lower crust (e.g., adakitic rocks in northern, central and southern Tibet) (e.g., Chung et al., 2003, 2005; Wang et al., 2005, 2008) and mantle (e.g., potassic and ultra-potassic rocks) (Turner et al., 1993; Chung et al., 1998, 2005; Ding et al., 2003).

Of particular interest are Miocene-Quaternary (18.0–1.5 Ma) lavas in the Hohxil area, northern margin of Tibet. The three end-member sources discussed above, contributed to petrogenesis of these lavas (Wang et al., 2005, 2012). This therefore provides an excellent opportunity to assess whether sediment recycling took place in the convergent margin. In this study, we present detailed B as well as Nd-Hf-Pb isotopic data for the Hohxil lavas, which suggests that subducted continental sediments entered the mid-to-lower crust and mantle and were subsequently recycled to the continental crust via magmatism. These findings confirm that the recycling of subducted sediments plays an important role in the differentiation of the continental crust (Plank and Langmuir, 1993; Hawkesworth et al., 1997; Chauvel et al., 2008; Behn et al., 2011; Liu and Rudnick, 2011; Marschall and Schumacher, 2012).

2. Geological background

The Himalayan-Tibetan Orogen mainly comprises the Qaidam-Kunlun, Songpan–Ganzi, Qiangtang, Lhasa and Himalayan blocks (Yin and Harrison, 2000; Chung et al., 2005) (Fig. 1a). The Songpan–Ganzi Block is bounded by the Jinshajiang suture to the south, and the Anyimaqen–Kunlun–Muztagh suture to the north (Yin and Harrison, 2000). The exposed Songpan–Ganzi Block consists mainly of Triassic and younger strata with some Mesozoic granites exposed in the central–eastern region (Yin and Harrison, 2000) and some Miocene-Quaternary volcanic rocks in the central–western region (Chung et al., 2005). The magmatic rocks investigated in this study are exposed as volcanic domes or lava sheets in six distinct areas within the Hohxil district, situated in the central Songpan–Ganzi Block. Specifically, these rocks comprise the southern Malanshan and Bukadaban biotite rhyolites, the Hudongliang tourmaline-bearing mica rhyolites, the western Wuxuefeng trachyandesites, the Hongshuihe dacites, and the southern Hohxil Lake olivine leucitites

(Fig. 1b). Notably, all of these volcanic rocks unconformably overlie Lower Triassic, Lower Cretaceous, or Tertiary strata (Wang et al., 2005; Qi et al., 2020).

The tourmaline-bearing mica and biotite rhyolites, which have a strong peraluminous composition, were generated between 9.0–1.5 Ma (Wang et al., 2012). The southern Malanshan biotite rhyolitic porphyries are characterized by phenocrysts of potassium feldspar, plagioclase, biotite, and quartz, whereas the Hudongliang tourmaline-bearing two-mica rhyolites contain phenocrysts of potassium feldspar, albite, biotite, quartz, muscovite, and tourmaline (Figs. 2a, b). The Bukadaban biotite rhyolites also have phenocrysts of potassium feldspar, plagioclase, biotite, and quartz (Fig. 2c). The groundmass of these rocks has a microlitic mineral composition that is similar to the phenocrysts and may contain cryptocrystalline-glassy materials. It has been suggested that these peraluminous felsic rocks were derived from mid-to-lower crustal sedimentary rocks (Wang et al., 2012).

The dacites and trachyandesites, which were generated between 18–15 Ma, have an adakitic composition resulting from partial melting of thickened eclogitic lower crust (Wang et al., 2005). The trachyandesites in western Wuxuefeng are characterized by porphyritic or glomeroporphyritic textures, with abundant phenocrysts surrounded by a fine-grained trachytic groundmass. The major phenocryst phases include potassium feldspar, plagioclase, clinopyroxene, and amphibole, while the groundmass is composed of a combination of potassium feldspar, clinopyroxene, plagioclase, biotite, and Fe-Ti oxides (Fig. 2d). Similarly, the Hongshuihe dacites consist of phenocrysts of potassium feldspar, plagioclase, amphibole, and quartz, embedded in a cryptocrystalline-glassy groundmass (Fig. 2e).

The olivine leucitites from southern Hohxil Lake were generated at ca. 16 Ma and originated from enriched mantle metasomatized by subducted sediments during southward subduction of the Asian continent (Wang et al., 2005; Qi et al., 2020). These rocks exhibit a characteristic porphyritic texture, with prominent phenocrysts of olivine, leucite, and clinopyroxene, and a microlitic to cryptocrystalline groundmass. The olivine and leucite phenocrysts are euhedral in shape and range in size from 0.2 to 1.5 mm (Fig. 2f). The groundmass of these rocks is composed of clinopyroxene, leucite, nepheline, titanomagnetite, sodalite, and apatite.

3. Results

We analyzed 18 whole-rock B isotopes, 16 whole-rock Hf isotopes, and 13 whole-rock Pb isotopes from Miocene-Quaternary lavas in the Hohxil area, and combined this data with previously published Nd-Pb isotopic data (Wang et al., 2005, 2012; Qi et al., 2020) to create a complete B-Hf-Nd-Pb isotope dataset. The analytical methods and all the isotopic data are listed in Supplementary data Text S1 and Tables S1–S2.

All Miocene–Quaternary lavas in the Hohxil area have high B contents and negative $\delta^{11}B$ values close to those of continental sediments (Fig. 3). Peraluminous rhyolites have the highest B (93–1559 ppm) contents with negative $\delta^{11}B$ (−9.7 to −17.9) values. The adakitic lavas exhibit the lowest B (18–29 ppm) contents with clearly negative $\delta^{11}B$ (−12.0 to −35.7) values, and the potassic olivine leucitites have B contents (37.2 to 59.3 ppm) and $\delta^{11}B$ (−8.3 to −15.6) values broadly intermediate between the other two groups (Table S1). All of the rocks also exhibit enriched Pb-Nd-Hf isotopic compositions comparable to the sediments (Fig. 4). They have similar $^{206}Pb/^{204}Pb$ (18.56–18.75), $^{207}Pb/^{204}Pb$ (15.49–15.72) and $^{208}Pb/^{204}Pb$ (38.31–39.01) ratios (Table S2). Strongly peraluminous rhyolites have the lowest $\varepsilon_{Nd}(t)$ (−5.83 to −7.41) and $\varepsilon_{Hf}(t)$ (−0.61 to −5.14) values, adakitic lavas exhibit consistent $\varepsilon_{Nd}(t)$ (−1.80 to −4.30) and $\varepsilon_{Hf}(t)$ (−0.36 to 0.16), and potassic olivine leucitites have similar $\varepsilon_{Nd}(t)$ (−3.07 to −3.89) and $\varepsilon_{Hf}(t)$ (0.23 to 1.08) values (Table S2).

4. Discussion

4.1 The relationships between B and Th, Nd, Pb and Hf

As mentioned above, a "paradox" exists between Nd-Hf-Pb and B isotopic compositions for arc magmatic rocks. We suggest that this "paradox" is caused by the geochemical differences between Nd-Hf-Pb and B. Boron is highly soluble in aqueous fluids at low temperatures, while the light rare elements (LREEs: La, Ce and Nd) and high field-strength elements (HFSEs: Nb, Ta, Zr, Th and Hf) are relatively immobile in aqueous fluids (Leemn and Sisson, 1996; Hawkesworth et al., 1997). The situation with Pb is a bit more complex because Pb^{2+} can be soluble in aqueous fluids, but Pb^{4+} behaves in a similar manner to HFSEs and is immobile in aqueous fluids. During subduction, some B may be lost from subducting slab and enter subduction-related fluids prior to the melting of the subducting AOC and sediments at high temperatures (Leeman and Sisson, 1996; Rose et al., 2001; Clift et al., 2003), but Nd, Hf and Pb remain in the subducting slab and do not enter the subduction-related fluids until temperatures exceed the solidus and initiate partial melting of the slab.

In addition, at high magmatic temperatures, B isotopes do not fractionate significantly and are likely to reflect source compositions (Palmer et al., 1992; Chaussidon and Marty, 1995). However, in subduction zones, the source compositions of arc magmatic rocks are complex, and include fluids or melts from the subducting AOC, sediments, and mantle wedge peridotites. Moreover, subduction-related fluid-triggered melting of mantle wedge peridotites or the interaction between subduction-related melts and mantle wedge peridotites results in substantial amounts of mantle wedge peridotite material contributing to the source of arc magmatic rocks. Boron and its isotopes in arc magmatic rocks are considered to resemble those of major fluid reservoirs, such as AOC or slab sediments (Morris et al., 1990; Edwards et al., 1993; Ishikawa and Nakamura, 1994; Leeman and Sisson, 1996; Smith et al., 1997; Clift et al., 2003). In contrast, Nd-Pb or Hf isotopes in arc rocks are likely to broadly reflect mantle wedge compositions (e.g., Edwards et al., 1993) or melt compositions from subducting sediments or oceanic crust if the subducting slab has melted (Kay et al., 1978; Plank and Langmuir, 1993; Hawkesworth et al., 1997; Shimoda et al., 1998; Chauvel et al., 2008; Behn et al., 2011).

Unlike magmatic arc rocks the magmatic rocks from continental collisional zones (e.g., the Himalayan-Tibetan Orogen) may contain some rocks directly derived by partial melting of crustal sedimentary rocks (e.g., tourmaline-bearing leucogranites or strongly peraluminous rhyolites), which can provide important information on the relationship between B and other elements (Th, Nd, Pb and Hf) during partial melting of continental sediments (Figs.

5 and 6). In the Hohxil area, Miocene-Quaternary (9.0–1.5 Ma) strongly peraluminous rhyolites were generated by partial melting of mid-crustal sedimentary rocks (Wang et al., 2012). The geochemical similarities (i.e., their incompatibility) of B, Pb and Th result in their enrichment in sediments, and allow Pb and Th to readily enter melts, while B enters melts or fluids during sediment melting (Kay et al., 1978; White et al., 1986; Morris et al., 1990; Plank and Langmuir, 1993; Leeman and Sisson, 1996; Hawkesworth et al., 1997). However, unlike B, Th is only mobilized in the sediment component (Hawkesworth et al., 1997). Thus, for the Hohxil strongly peraluminous rhyolites, the negative correlation between Th and B contents (Fig. 5a) indicates geochemical differences during sediment melting.

High B/Nb and Th/Nb ratios are likely to indicate predominantly sediment-derived aqueous fluid (Ishikawa and Nakamura, 1994) and sediment-derived melt components (Hawkesworth et al., 1997), respectively. Thus, the Th/Nb vs B/Nb diagram can help reveal the trends of sediment melting and aqueous fluid for the Hohxil strongly peraluminous rhyolites (Fig. 4b), which suggests that both sediment-derived fluids and melts played a critical role in their petrogenesis. The negative correlations between B and Nd, Pb and Hf (Fig. 5c, e and g), and the two composition trends in Nd/Nb, Pb/Nd and Hf/Nb vs B/Nb space (Fig. 5d, f and h) suggest that Nd, Pb and Hf have geochemical characteristics similar to Th during sediment melting, thus providing further evidence of the contributions of both sediment-derived fluids and melts in the formation of the Hohxil strongly peraluminous rhyolites.

Based on detailed studies of elemental and Sr-Nd-Pb-Hf geochemistry, as well as experimental petrology data (Fig. 4a-c), the Hohxil strongly peraluminous rhyolites are considered to have been generated by dehydration melting of muscovite- and biotite-bearing sedimentary rocks (Wang et al., 2012). As B is primarily hosted by micas and clay minerals in silicic rocks (Leeman and Sisson, 1996), it can easily enter sediment-derived fluids and melts due to its incompatibility during dehydration melting. The Hohxil strongly peraluminous rhyolites exhibit negative $\delta^{11}B$ (−9.7 to −17.9) values, similar to continental sediments, and B (93–1559 ppm), B/Zr (1–27) and B/Ce (1–70) values close to, or slightly higher than, those of continental or marine sediments (Figs. 3 and 6). This confirms that B behaves as an incompatible trace element, preferentially residing in fluids and melts during sediment melting (Leeman and Sisson, 1996).

Furthermore, the rhyolites in this study have high B contents similar to those of leucogranites from the Himalayas, the Tuscan (Italy) magmatic province, strongly peraluminous rhyolites from the Spor Mountain and Honeycomb Hills (Utah, USA), Taylor Greek (SW New Mexico) and Macusani (Peruvian Andes). All of these rocks formed in areas characterized by significant crustal thickening (Leeman and Sisson, 1996). This indicates that significant B enrichment in their sedimentary source regions (Leeman and Sisson, 1996). For the Hohxil strongly peraluminous rhyolites and the Himalaya leucogranites in the northern and southern margins of Tibet, respectively, the most likely source rocks are sedimentary rocks that entered the mid-to-lower crust during crustal thickening by the subduction or underthrusting of continental crust (e.g., Searle et al., 1997; Guo and Wilson, 2012; Wang et al., 2012). Furthermore, in the northern margin of Tibet, the B-Pb isotope systematics of the Hohxil strongly peraluminous rhyolites (Figs. 3 and 4d) suggest that such sedimentary rocks are likely to be of continental affinity.

4.2 Subducted continental sediments entered the eclogites-facies lower crust

The discovery of the relationship between B and Th, Nd, Pb and Hf during sediment melting may help to further constrain the petrogenesis of the Hohxil Miocene adakitic lavas. Based on element and Sr-Nd isotopic data, these adakitic rocks were considered to have been generated by partial melting of eclogitic lower crust thickened by continental subducting (Wang et al., 2005). However, the new data for whole rock Pb-Hf, as well as Nd isotopes, further indicate that the adakitic rocks clearly contain a sediment component (Fig. 4a-c). They have more negative $\delta^{11}B$ (−12.0 to −35.7) values, and lower B (18–29 ppm) contents than those of the Hohxil strongly peraluminous rhyolites. Added to this, their B contents are close to, or slightly lower than, those of continental or marine sediments (Figs. 3 and 6), but similar to the average value (20 ppm) of continental upper crust and are clearly higher than the average values (1.0, ~ 0.1 and < 0.05 ppm) of continental lower crust, primitive mantle and depleted mantle, respectively (Fig. 6b) (Chaussidon and Marty, 1995; Leeman and Sisson, 1996).

B-Pb isotope systematics (Figs. 3 and 4d) suggest the source of these adakitic rocks should contain continental-affinity rocks. However, they also exhibit Nb/Ta (15–21) and B/Ce (0.08–0.13) ratios similar to those of mantle (Fig. 6) (Leeman and Sisson, 1996; Rudnick et al., 2000; Wang et al., 2005), but different from those (3–10 and 1.0–70) of the Hohxil strongly peralumious rhyolites (Fig. 6) (Wang et al., 2012). This indicates that their source region also contained a mafic component from mantle, in addition to a continental sediment component. They have the lowest B contents (Figs. 3 and 5) among Miocene-Quaternary crust and mantle-derived magmatic rocks in the Hohxil area, suggesting that they could not be generated by mixing between crust- and mantle-derived magmas. Therefore, the mafic endmember component of the source region of adakitic rocks is likely to be mafic rocks in the lower crust rather than mafic magmas entering the lower crust. These adakitic rocks are likely to be derived by partial melting of this mixed source with meta-mafic and sedimentary rocks under eclogite-facies conditions (Wang et al., 2005). The metasedimentary rocks possibly entered the lower crust through continental subduction, as suggested by previous investigations in petrology, geochemistry, numerical modelling, and geophysics (e.g., Willett and Beaumont, 1994; Hacker et al., 2000, 2012; Yin and Harrision, 2000; Tapponnier et al., 2001; Kind et al., 2002; Kapp et al., 2003; McKenzie and Priestley, 2008; Zhao et al., 2010, 2011; Huangfu et al., 2018; Ma et al., 2021; Hao et al., 2022).

Prograde metamorphism and accompanying dehydration of subducting continental crust at lower crust to mantle depths may cause B isotopic fractionation similar to that of a subducting oceanic slab. This is because dehydration of a subducting oceanic slab extracts B into the fluid and leaves residues that are depleted in B (Rose et al., 2001). Some studies have shown that $\delta^{11}B$ of dehydration residues (prograde metamorphic rocks) become progressively lighter with increasing degrees of dehydration (Moran et al., 1992; Bebout et al., 1993; Peacock and Hervig, 1999; Nakano and Nakamura, 2001; Rose et al., 2001). Therefore, the dehydration process results in increasingly lower B concentrations and increasingly light B isotopic compositions in both residual rock and instantaneous fluid

(Rose et al., 2001). Eclogitic lower crust-derived adakitic rocks have the lowest B contents and some samples also have the lowest $\delta^{11}B$ values (Figs. 3, 5 and 6) among Miocene-Quaternary crust and mantle-derived magmatic rocks in the Hohxil area. This indicates that their sources may have undergone B isotopic fractionation during dehydration and eclogites-facies metamorphism. Consequently, their sources (subducted sediment-bearing continental crust) should have lower B contents and $\delta^{11}B$ values than those of source rocks for the Hohxil strongly peraluminous rhyolites.

4.3 Mantle metasomatized by subducted continental sediments

Mantle-derived olivine leucitites were likely generated by partial melting of mantle that was metasomatized by subducted sediment-bearing eclogitic continental crust-derived melts or fluids. Generally, mantle has low B contents ($\leq$ 0.1–0.05 ppm), which lead to mantle-derived magmas with low B contents ($\leq$ 1 ppm) (Chaussidon and Marty, 1995). However, the leucitites in this study exhibit relatively high B (37 to 59 ppm) contents with negative $\delta^{11}B$ (−8.3 to −15.6) values, similar to those of continental or marine sediments, or the continental upper crust (Figs. 3 and 6). This suggests that these leucitites may be derived from mantle that was enriched by subducted sediments. They have Nd-Hf-B isotope compositions broadly similar to eclogitic lower crust-derived adakitic rocks (Figs. 3 and 4). Additionally, both leucitites and adakitic rocks exhibit many similar trace element geochemical characteristics (Figs. 5 and 6), indicating a sediment melt composition trend (Figs. 5 and 6). Therefore, we suggest that the leucitites were likely generated by partial melting of mantle that was metasomatized by subducted sediment-bearing eclogitic lower crust-derived melts and/or fluids. Nevertheless, the leucitites exhibit clearly higher B contents than those of the adakitic rocks (Fig. 3). It is worth noting that subducting continental crust-derived melts and/or fluids could metasomatize portions of the upper mantle and induce melting to produce B-rich and high $\delta^{11}B$ magmas.

5. Conclusions

1) Evidence based on B-Hf-Pb-Nd isotopes of Miocene–Quaternary lavas in the northern margin of Tibet indicates that subducted continental sediments entered the mid-to-lower crust and mantle, and then were recycled to the continental crust via magmatism.
2) The strongly peraluminous rhyolites with the highest B contents were generated by partial melting of mica-bearing continental sedimentary rocks at mid-to-lower crustal depths.
3) The adakitic lavas with the lowest B contents were derived by partial melting of sediment-bearing thickened lower crust at eclogites-facies conditions.
4) The olivine leucitites with intermediate B contents were generated by partial melting of mantle metasomatized by sediment-bearing eclogitic continental crust-derived melts.
5) Our new results indicate that the recycling of subducted sediments plays an important role in the differentiation of the continental crust at continental convergent margins.

Acknowledgments

This study was supported by the Second Tibetan Plateau Scientific Expedition and

Research program (2019QZKK0702) and the National Natural Science Foundation of China (Nos. 42021002, 41872065, and 91855215). This is contribution No. IS–XXXX from GIGCAS.

References

Arndt, N.T., Goldstein, S.L., 1989. An open boundary between lower continental crust and mantle: Its role in crust formation and crustal recycling. Tectonophysics 161, 201–212.

Atherton, M.P., Petford, N., 1993. Generation of sodium-rich magmas from newly underplated basaltic crust. Nature 362, 144–146.

Bebout, G.E., Ryan, J.G., Leeman, W.P., 1993. B-Be systematics in subduction-related metamorphic rocks: Characterization of the subducted component. Geochim. Cosmochim. Ac. 57(10), 2227–2237.

Behn, M.D., Kelemen, P.B., Hirth, G., Hacker, B.R., Massonne, H.J., 2011. Diapirs as the source of the sediment signature in arc lavas. Nature Geoscience 4(9), 641–646.

Chaussidon, M., Albarède, F., 1992. Secular boron isotope variations in the continental crust: an ion microprobe study. Earth Planet. Sci. Lett. 108(4), 229–241.

Chauvel, C., Lewin, E., Carpentier, M., Arndt, N.T., Marini, J.C., 2008. Role of recycled oceanic basalt and sediment in generating the Hf-Nd mantle array. Nat. Geosci. 1(1), 64–67.

Chung, S.L., Lo, C.H., Lee, T.Y., Zhang, Y., Xie, Y., Li, X., Wang, K.L., Wang, P.L., 1998. Diachronous uplift of the Tibetan plateau starting 40 Myr ago. Nature 394(6695), 769–773.

Chung, S.L., Liu, D.Y., Ji, J.Q., Chu, M.F., Lee, H.Y., Wen, D.J., Lo, C.H., Lee, T.Y., Qian, Q., Zhang, Q., 2003. Adakites from continental collision zones: Melting of thickened lower crust beneath southern Tibet. Geology 31, 1021–1024.

Chung, S.L., Chu, M.F., Zhang, Y., Xie, Y., Lo, C.H., Lee, T.Y., Lan, C.Y., Li, X., Zhang, Q., Wang, Y., 2005. Tibetan tectonic evolution inferred from spatial and temporal variations in post-collisional magmatism. Earth-Sci. Rev. 68(3–4), 173–196.

Clift, P.D., Layne, G.D., Najman, Y.M.R., Kopf, A., Shimizu, N., Hunt, J., 2003. Temporal Evolution of Boron Flux in the NE Japan and Izu Arcs Measured by Ion Microprobe from the Forearc Tephra Record. J. Petrol. 44(7), 1211–1236.

Defant, M.J. Drummond, M.S., 1990. Derivation of some modern arc magmas by melting of young subducted lithosphere. Nature 347, 662–665.

De Hoog, J.C.M., Savov, I.P., 2018. Boron Isotopes as a Tracer of Subduction Zone Processes. In: Marschall, H., Foster, G. (Eds.) Boron Isotopes: The Fifth Element. Advances in Isotope Geochemistry. Springer International Publishing, Cham, 217–247.

Ding, L., Kapp, P., Zhong, D., Deng, W., 2003. Cenozoic Volcanism in Tibet: Evidence for a Transition from Oceanic to Continental Subduction. J. Petrol. 44(10), 1833–1865.

Edwards, C.M.H., Morris, J.D., Thirlwall, M.F., 1993. Separating mantle from slab signatures in arc lavas using B/Be and radiogenic isotope systematics. Nature 362, 530–533.

Gazel, E., Hayes, J. L., Hoernle, K., Kelemen, P., Everson, E., Holbrook, W.S., Hauff, F., Van Den Bogaard, P., Vance, E.A., Chu, S., Calvert, A.J., Carr, M.J., Yogodzinski, G.M., 2015. Continental crust generated in oceanic arcs. Nat. Geosci. 8(4), 321–327.

Guo, Z., Wilson, M., 2012. The Himalayan leucogranites: Constraints on the nature of their crustal source region and geodynamic setting. Gondwana Res. 22(2), 360–376.

Hacker, B.R., Gnos, E., Ratschbacher, L., Grove, M., Mcwilliams, M., Sobolev, S.V., Wan, J., Wu, Z.H., 2000. Hot and dry deep crustal xenoliths from Tibet. Science 287(5462), 2463–2466.

Hacker, B.R., Kelemen, P.B., Behn, M.D., 2011. Differentiation of the continental crust by relamination. Earth Planet. Sci. Lett. 307(3–4), 501–516.

Hao, LL., Wang, Q., Kerr, A., Wei, GJ., Huang, F., Zhang, MY., Qi, Y., Ma, L., Chen, XF., Yang, Y.N., 2022. Contribution of continental subduction to very light B isotope signatures in post-collisional magmas: evidence from southern Tibetan ultrapotassic rocks. Earth Planet. Sci. Lett. 584, 117508

Hawkesworth, C.J., Kemp, A.I.S., 2006. Evolution of the continental crust. Nature 443(7113), 811–817.

Hawkesworth, C.J., Turner, S.P., Mcdermott, F., Peate, D.W., Van Calsteren, P., 1997. U-Th isotopes in arc magmas: Implications for element transfer from subducted crust. Science 276, 561–555.

Huangfu, P., Li, Z.-H., Gerya, T., Fan, W., Zhang, K.-J., Zhang, H., Shi, Y., 2018. Multi-terrane structure controls the contrasting lithospheric evolution beneath the western and central–eastern Tibetan plateau. Nat. Commun. 9, 3780.

Ishikawa, T., Nakamura, E., 1994. Origin of the slab component in arc lavas form across-arc variation of B and Pb isotopes. Nature 370, 205–208.

Jull, M., Kelemen, P.B.. 2001. On the conditions for lower crustal convective instability.

J. Geophys. Res-Sol. Ea. 106, 6423–6446.

Kapp, P., Murphy, M.A., Yin, A., Harrison, T.M., Ding, L., Guo, J., 2003. Mesozoic and Cenozoic tectonic evolution of the Shiquanhe area of western Tibet. Tectonics 22, 1029, doi: 1010.1029/2001TC001332.

Kay, R.W., Kay, S.M., 1993. Delamination and delamination magmatism. Tectonophysics 219, 177–189.

Kay, R.W., Sun, S.S., Lee-Hu, C.N., 1978. Pb and Sr isotopes in volcanic rocks from the Aleutian Islands and Pribilof Islands, Alaska. Geochim. Cosmochim. Ac. 42, 263–273.

Kemp, A.I.S., Hawkesworth, C.J., Foster, G.L., Paterson, B.A., Woodhead, J.D., Hergt, J.M., Gray, C.M., Whitehouse, M.J., 2007. Magmatic and crustal differentiation history of granitic rocks from Hf-O isotopes in zircon. Science 315(5814), 980–983.

Kind, R., Yuan, X., Saul, J., Nelson, D., Sobolev, S.V., Mechie, J., Zhao, W., Kosarev, G., Ni, J., Achauer, U., Jiang, M., 2002. Seismic images of crust and upper mantle beneath Tibet: Evidence for Eurasian plate subduction. Science 298(5596), 1219–1221.

Knesel, K.M., Davidson, J.P., 2002. Insights into collisional magmatism from isotopic fingerprints of melting reactions. Science 296(5576), 2206–2208.

Lee, C.T.A., Morton, D.M., Little, M.G., Kistler, R., Horodyskyj, U.N., Leeman, W.P., Agranier, A., 2008. Regulating continent growth and composition by chemical weathering. Proc. Natl. Acad. Sci. 105(13), 4981–4986.

Leeman W.P. Sisson V.B., 1996. Geochemistry of boron and its implications for crustal and mantle processes. Boron: Mineralogy, Petrology and Geochemistry (Grew, E. S. and Anovitz, L. M., eds.), Rev. Mineral. 33, 645–708.

Liu, X.M., Rudnick, R.L., 2011. Constraints on continental crustal mass loss via chemical weathering using lithium and its isotopes. Proc. Natl. Acad. Sci. 108(52), 20873–20880.

Ma, L., Gou, G.N., Kerr, A.C., Wang, Q., Wei, G.J., Yang, J.H., Shen, X.M., 2021. B isotopes reveal Eocene mélange melting in northern Tibet during continental subduction. Lithos 392-393, 106146

Marschall, H.R., Schumacher, J.C., 2012. Arc magmas sourced from melange diapirs in subduction zones. Nat. Geosci. 5(12), 862–867.

McKenzie, D., Priestley, K.. 2008. The influence of lithospheric thickness variations on continental evolution. Lithos 102, 1–11.

Moran, A.E., Sisson, V.B., Leeman, W.P., 1992. Boron depletion during progressive metamorphism: Implications for subduction processes. Earth Planet. Sci. Lett. 111(2–4), 331–349.

Morris, J.D., Leeman, W.P., Tera, F., 1990. The subducted component in island arc lavas constraints from Be isotopes and B-Be systematics. Nature 344, 31–36.

Nábelek, J., Hetényi, G., Vergne, J., Sapkota, S., Kafle, B., Jiang, M., Su, H., Chen, J., Huang, B.S., Team, T.H.C., 2009. Underplating in the Himalaya-Tibet Collision Zone Revealed by the Hi-CLIMB Experiment. Science 325(5946), 1371–1374.

Nakano, T., Nakamura, E., 2001. Boron isotope geochemistry of metasedimentary rocks and tourmalines in a subduction zone metamorphic suite. Phys. Earth Planet. In. 127(1–4), 233–252.

Palmer, M.R., London, D., Morgan, G.B., Babb, H.A., 1992. Experimental determination of fractionaltion of $^{11}B/^{10}B$ between tourmaline and aqueous vapour: a temperature and pressure dependenr isotopic system. Chem. Geol. (Isotope Geoscience Section) 101, 123–130.

Palmer, M.R., 1991. Boron-isotope systematics of Halmahera arc (Indonesia) lavas: Evidence for involvement of the subducted slab. Geology 19, 215–217.

Palmer, M.R., 2017. Boron cycling in subduction zones. Elements 13(4), 237–242.

Patiño Douce, A.E., Harris, N., 1998. Experimental constraints on Himalayan anatexis. J. Petrol. 39, 689–710.

Peacock, S.M., Hervig, R.L., 1999. Boron isotopic composition of subduction-zone metamorphic rocks. Chem. Geol. 160(4), 281–290.

Plank, T., Langmuir, C.H., 1993. Tracing trace elements from sediment input to volcanic output at subduction zones. Nature 362, 739–743.

Plank, T., Langmuir, C.H., 1998. The chemical composition of subducting sediment and its consequences for the crust and mantle. Chem. Geol. 145, 325–394.

Richards, A., Argles, T., Harris, N., Parrish, R., Ahmad, T., Darbyshire, F., Draganits, E., 2005. Himalayan architecture constrained by isotopic tracers from clastic sediments. Earth Planet. Sci. Lett. 236(3-4), 773–796

Rose, E.F., Shimizu, N., Layne, G.D., Grove, T.L., 2001. Melt Production Beneath Mt. Shasta from Boron Data in Primitive Melt Inclusions. Science 293(5528), 281–283.

Rudnick, R.L., 1995. Making continental crust. Nature 378, 571–578.

Qi, Y., Wang, Q., Zhu, Y.T., Shi, L.C., Yang, Y.N., 2020. Miocene olivine leucitites in the Hoh Xil basin, northern Tibet: implications for intracontinental lithosphere melting and surface uplift of the Tibetan Plateau. J. Petrol. 61, 1–18

Searle, M.P., Parrish, R.R., Hodges, K.V., Hurford, A., Ayres, M.W., Whitehouse, M.J.,

1997. Shisha Pangma Leucogranite, South Tibetan Himalaya: Field Relations, Geochemistry, Age, Origin, and Emplacement. J. Petrol. 105(3), 295–318.

Shen, B., Jacobsen, B., Lee, C.T.A., Yin, Q.Z., Morton, D.M., 2009. The Mg isotopic systematics of granitoids in continental arcs and implications for the role of chemical weathering in crust formation. Proc. Natl. Acad. Sci. 106(49), 20652–20657.

Shimoda, G., Tatsumi, Y., Nohda, S., Ishizaka, K., Jahn, B.M., 1998. Setouchi high-Mg andesites revisited: geochemical evidence for melting of subducting sediments. Earth Planet. Sci. Lett. 160(3-4), 479–492.

Smith, H.J., Leeman, W.P., Davidson, J., Spivack, A.J., 1997. The B isotopic composition of arc lavas from Martinique, Lesser Antilles. Earth Planet. Sci. Lett. 146(1–2), 303–314.

Tapponnier, P., Xu, Z., Roger, F., Meyer, B., Arnaud, N., Wittlinger, G., Yang, J., 2001. Oblique stepwise rise and growth of the Tibet Plateau. Science 294(5547), 1671–1677.

Taylor, S.R., McLennan, S.M., 1985. The Continental Crust: Its Composition and Evolution. Blackwell, Oxford.

Turner, S., Hawkesworth, C., Liu, J., Rogers, N., Kelley, S., van Calsteren, P., 1993. Timing of Tibetan uplift constrained by analysis of volcanic rocks. Nature 364, 50–54.

Wang, Q., Mcdermott, F., Xu, J.F., Bellon, H., Zhu, Y.T., 2005. Cenozoic K-rich adakitic volcanic rocks in the Hohxil area, northern Tibet: Lower-crustal melting in an intracontinental setting. Geology 33(6), 465–468.

Wang, Q., Wyman, D.A., Xu, J., Dong, Y., Vasconcelos, P.M., Pearson, N., Wan, Y., Dong, H., Li, C., Yu, Y., Zhu, T., Feng, X., Zhang, Q., Zi, F., Chu, Z., 2008. Eocene melting of subducting continental crust and early uplifting of central Tibet: Evidence from central–western Qiangtang high-K calc-alkaline andesites, dacites and rhyolites. Earth Planet. Sci. Lett. 272, 158–171.

Wang, Q., Chung, S.L., Li, X.H., Wyman, D., Li, Z.X., Sun, W.D., Qiu, H.N., Liu, Y.S., Zhu, Y.T., 2012. Crustal Melting and Flow beneath Northern Tibet: Evidence from Mid-Miocene to Quaternary Strongly Peraluminous Rhyolites in the Southern Kunlun Range. J. Petrol. 53(12), 2523–2566.

Wang, D., Romer, R.L., Guo, J.H., Glodny, J., 2020. Li and B isotopic fingerprint of Archean subduction. Geochim. Cosmochim. Ac. 268, 446–466.

White, W.M., Dupr´e, B., Vidal, P., 1985. Isotope and trace element geochemistry of sediments from the Barbados Ridge-Demerara Plain region, Atlantic Ocean. Geochim. Cosmochim. Ac. 49, 1875–1886.

Willett, S.D., Beaumont, C., 1994. Subduction of Asian lithospheric mantle beneath Tibet inferred from models of continental collision. Nature 369(6482), 642–645.

Yamaoka, K., Ishikawa, T., Matsubaya, O., Ishiyama, D., Nagaishi, K., Hiroyasu, Y., Chiba, H., Kawahata, H., 2012. Boron and oxygen isotope systematics for a complete section of oceanic crustal rocks in the Oman ophiolite. Geochim. Cosmochim. Ac. 84(0), 543–559.

Yin, A., Harrison, T.M., 2000. Geologic evolution of the Himalayan–Tibetan orogen. Annu. Rev. Earth. Pl. Sc. 28, 211–280.

Zhao, J., Yuan, X., Liu, H., Kumar, P., Pei, S., Kind, R., Zhang, Z., Teng, J., Ding, L., Gao, X., Xu, Q., Wang, W., 2010. The boundary between the Indian and Asian tectonic plates below Tibet. Proc. Natl. Acad. Sci. 107, 11229–11233.

Zhao, W., Kumar, P., Mechie, J., Kind, R., Meissner, R., Wu, Z., Shi, D., Su, H., Xue, G., Karplus, M., Tilmann, F., 2011. Tibetan plate overriding the Asian plate in central and northern Tibet. Nat. Geosci. 4(12), 870–873.

Zindler, A., Hart, S., 1986, Chemical geodynamics: Annu. Rev. Earth. Pl. Sc. 14, 493–571.

Figure captions

Figure 1. (a) Geological sketch map of Tibet showing major blocks and temporal-spatial distribution of Cenozoic volcanic rocks (modified from Chung et al., 2005). Cenozoic volcanic rocks data are from Chung et al. (2003), Ding et al. (2003), and Wang et al. (2005). Main suture zones between major blocks: AKMS—Anymaqen–Kunlun–Muztagh Suture; JS—Jinsha Suture; BS—Bangong–Nujiang Suture; IS—Indus–Yarlung Zangbo Suture. Major faults: STDS—southern Tibet detachment system; MBT—Main Boundary thrust. (b) Simplified geologic map showing outcrops of magmatic rocks in Hohxil area, Songpan-Ganzi block, northern Tibet

Figure 2 Photomicrographs of the Miocene–Quaternary lavas. (a) The southern Malanshan biotite rhyolitic porphyries (sample 2303, crossed polarized light); (b) the Hudongliang tourmaline-bearing two-mica rhyolite (sample 1P2JD7-1, plane-polarized light); (c) the Bukadaban biotite rhyolite (sample 2303, crossed polarized light); (d) the western Wuxuefeng trachyandesites (sample 3302, plane-polarized light); (e) the Hongshuihe dacites (sample 3304-3b, crossed polarized light)；(f) the Hoh Xil olivine leucitites (sample 6304b, crossed polarized light). Ab = albite, Bt = biotite, Kf = potassium feldspar, Mus = muscovite, Pl = plagioclase, Qtz` = quartz, Tm = tourmaline, Ol = olivine, Amp =

amphibole, Cpx = clinopyroxene, Lec = leucite, Xe = nepheline; Ap = apatite; Tmt = titanomagnetite.

Figure 3 δ^{11}B–boron contents (B) diagram (modified from Rose et al., 2001). MORB—mid-ocean ridge basalts; OIB—ocean island basalts; AOC—altered oceanic crust; DMM—depleted MORB mantle. Striped fields for B reservoirs (MORB, OIB, AOC and DMM), as well as melt inclusions hosted by high-Mg olivines in basaltic andesite from Mt. Shasta and their potential source rock are from Rose et al. (2001) and references therein. The fields for continental sediments, marine sediments and arc lavas are after Leeman & Sisson (1996). The B-Pb data for Setouchi high-Mg andesites in Japan are from Ishikawa & Nakamura (1994).

Figure 4 (a) ^{206}Pb/^{204}Pb–^{207}Pb/^{204}Pb diagram. (b) ^{206}Pb/^{204}Pb–^{208}Pb/^{204}Pb diagram. (c) ε_{Nd}(t)–ε_{Hf}(t) diagram. (d) δ^{11}B–^{207}Pb/^{204}Pb diagram. NHRL: Northern Hemisphere Reference Line. EM1 and EM2: enriched mantle end-members (Zindler & Hart, 1986). The field for marine sediments is constructed using the data of Plank & Langmuir (1998). The fields for MORB, OIB and sediments (Fe–Mn crusts and nodules, subducted oceanic sediment, clays and biogenic muds, sands and Himalayan sediments) are after Richards et al. (2005), Chauvel et al. (2008) and references therein. The B-Nd-Pb-Hf data for Setouchi high-Mg andesites in Japan and AOC are from Ishikawa & Nakamura (1994) and Shimoda et al. (1998).

Figure 5 (a, c, e, g) B vs. Th, Nd, Pb, and Hf contents, respectively. (b, d, f, h) B/Nb vs.

Th/Nb, Nd/Nb, Pb/Nb, and Hf/Nb, respectively.

Figure 6 (a) B vs. B/Zr diagram. (b) B vs. B/Ce diagram. The data (averages) for pelagic clay (PC), upper crust (UC), and estimated primitive upper mantle (PUM) are from Taylor & Mclennan (1985). The fields for typical granulites, B-enriched granulites, sediments, peridotites, island arc lavas, and mantle B/Ce ratios are after Leeman & Sisson (1996) and references therein.

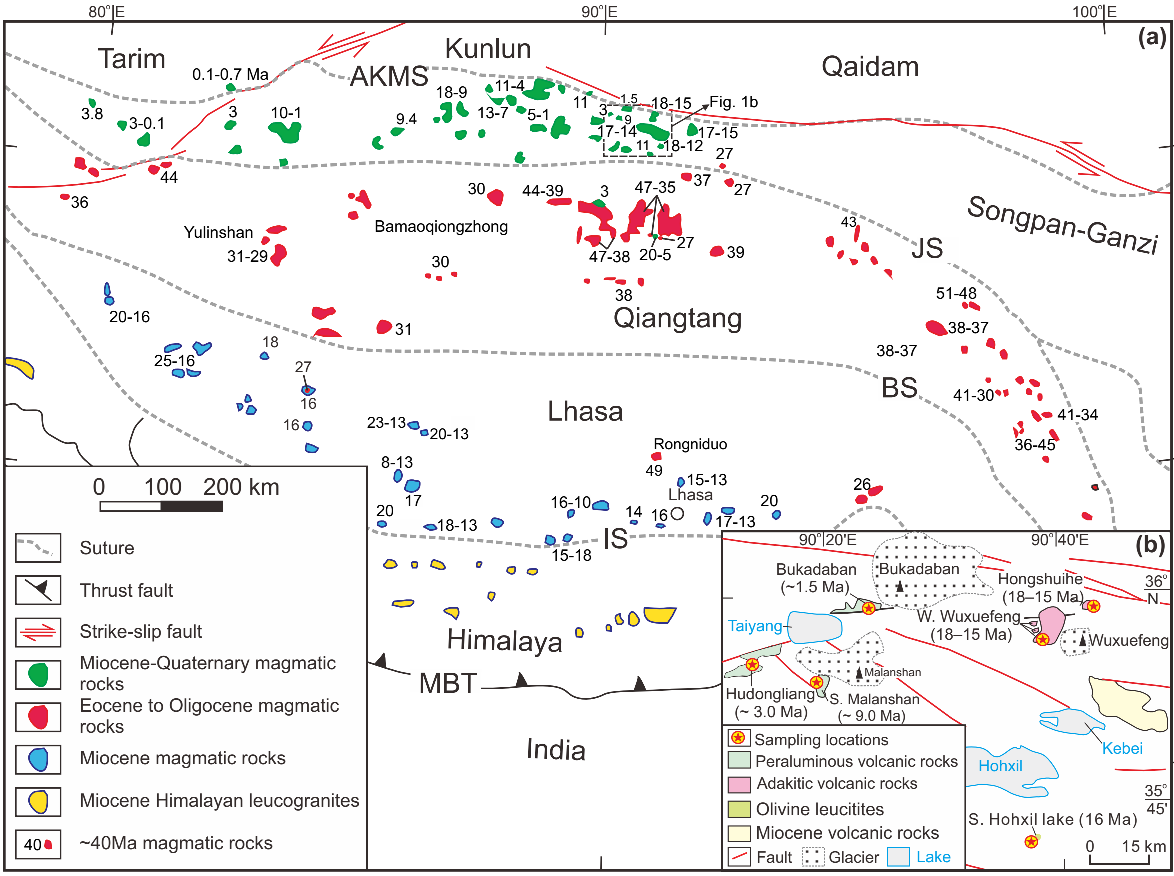

(a)
(b)
Tarim
Kunlun
Qaidam
AKMS
Songpan-Ganzi
JS
BS
Qiangtang
Lhasa
IS
Himalaya
MBT
India
Yulinshan
Bamaoqiongzhong
Rongniduo
Lhasa
Fig. 1b
0 100 200 km
Suture
Thrust fault
Strike-slip fault
Miocene-Quaternary magmatic rocks
Eocene to Oligocene magmatic rocks
Miocene magmatic rocks
Miocene Himalayan leucogranites
~40Ma magmatic rocks
Bukadaban (~1.5 Ma)
Hongshuihe (18–15 Ma)
W. Wuxuefeng (18–15 Ma)
Wuxuefeng
Taiyang
Malanshan
Hudongliang (~ 3.0 Ma)
S. Malanshan (~ 9.0 Ma)
Kebei
Hohxil
S. Hohxil lake (16 Ma)
Sampling locations
Peraluminous volcanic rocks
Adakitic volcanic rocks
Olivine leucitites
Miocene volcanic rocks
Fault
Glacier
Lake
0 15 km

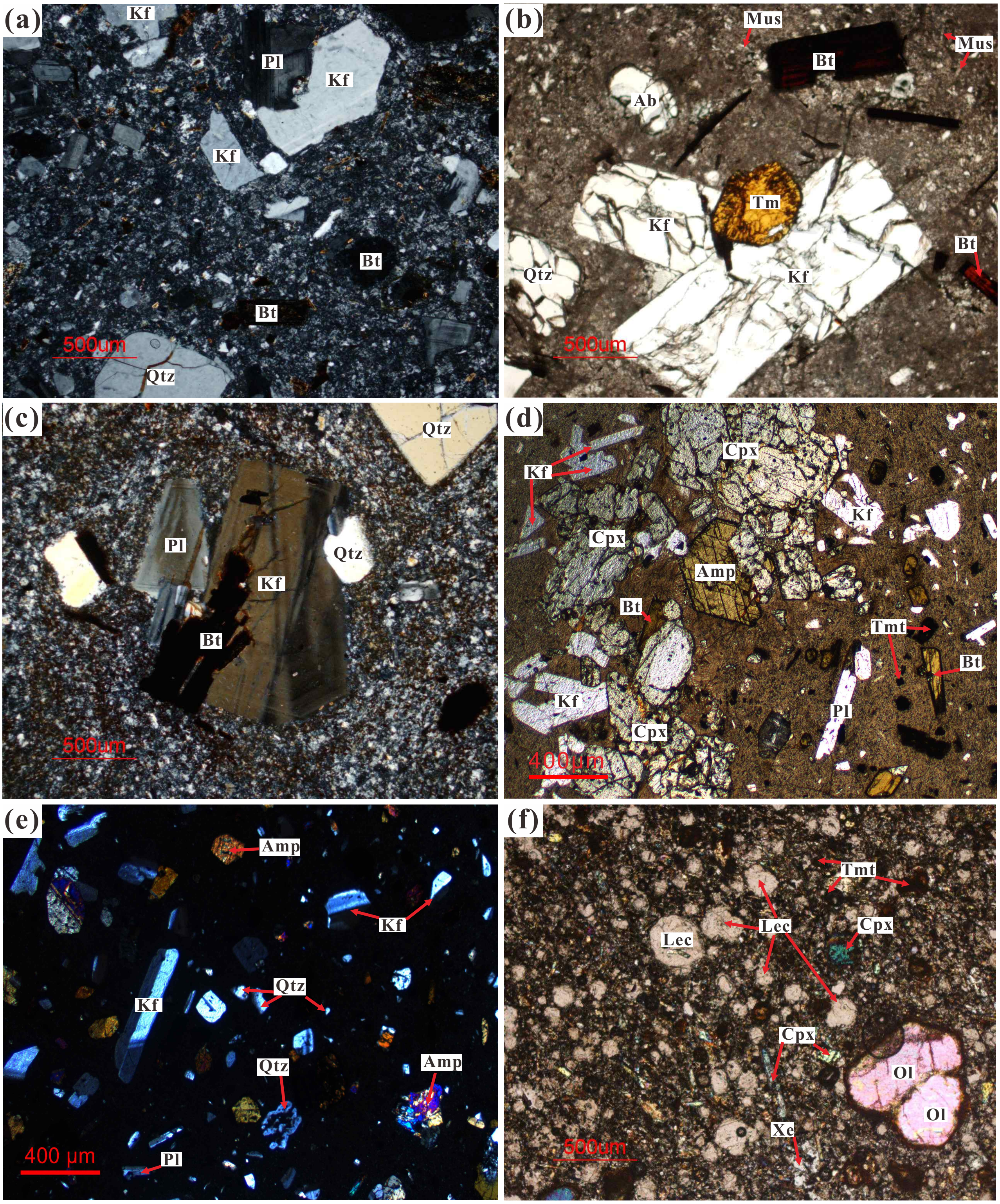

(a)
Kf
Pl
Kf
Kf
Bt
Bt
500um
Qtz
(b)
Mus
Bt
Mus
Ab
Tm
Kf
Kf
Qtz
Bt
500um
(c)
Qtz
Pl
Qtz
Kf
Bt
500um
(d)
Cpx
Kf
Kf
Cpx
Amp
Bt
Tmt
Bt
Kf
Pl
Cpx
400μm
(e)
Amp
Kf
Qtz
Kf
Qtz
Amp
400 μm
Pl
(f)
Tmt
Lec
Lec
Cpx
Cpx
Ol
Ol
Xe
500um

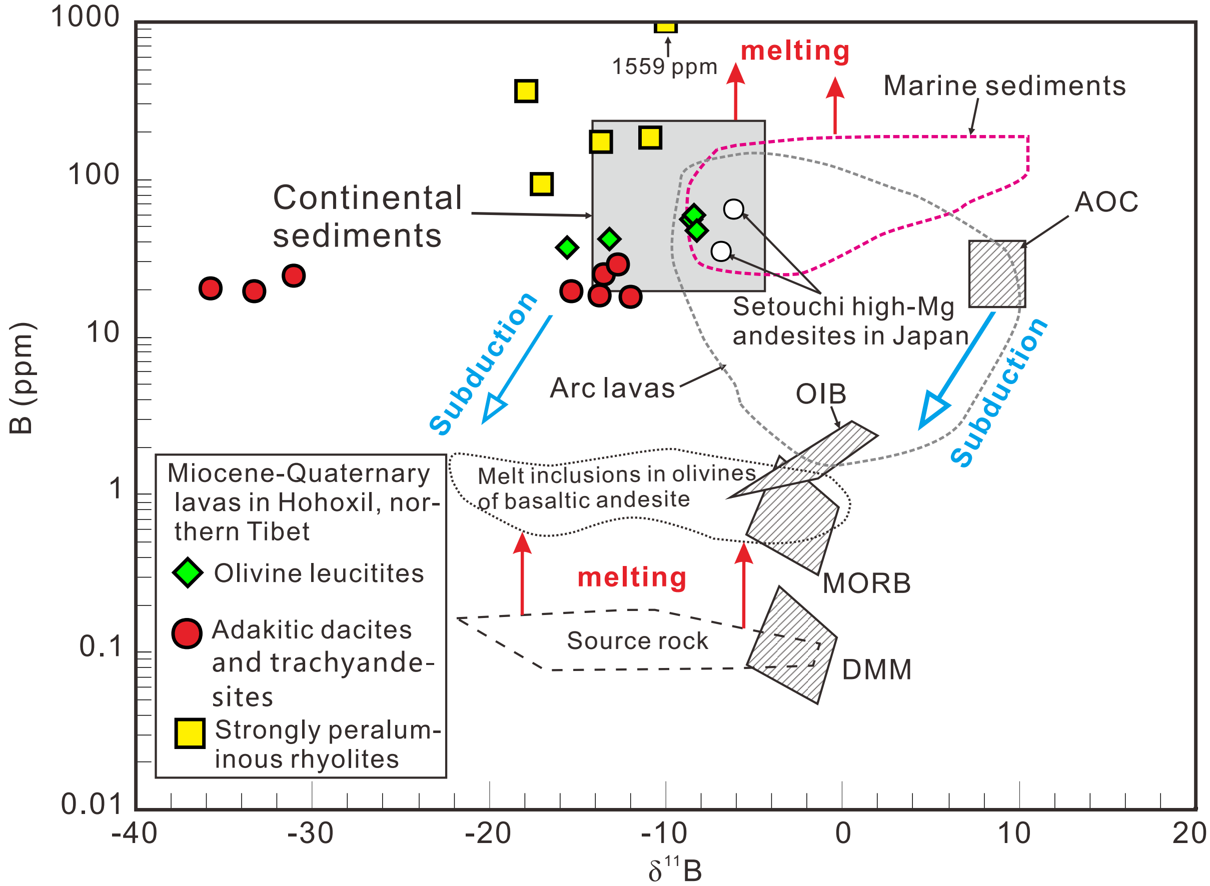
1000
100
10
1
0.1
0.01
B (ppm)
-40
-30
-20
-10
0
10
20
δ11B
1559 ppm
melting
Marine sediments
Continental
sediments
AOC
Setouchi high-Mg
andesites in Japan
Subduction
Arc lavas
OIB
Subduction
Miocene-Quaternary
lavas in Hohoxil, nor-
thern Tibet
Olivine leucitites
Adakitic dacites
and trachyande-
sites
Strongly peralum-
inous rhyolites
Melt inclusions in olivines
of basaltic andesite
MORB
melting
Source rock
DMM

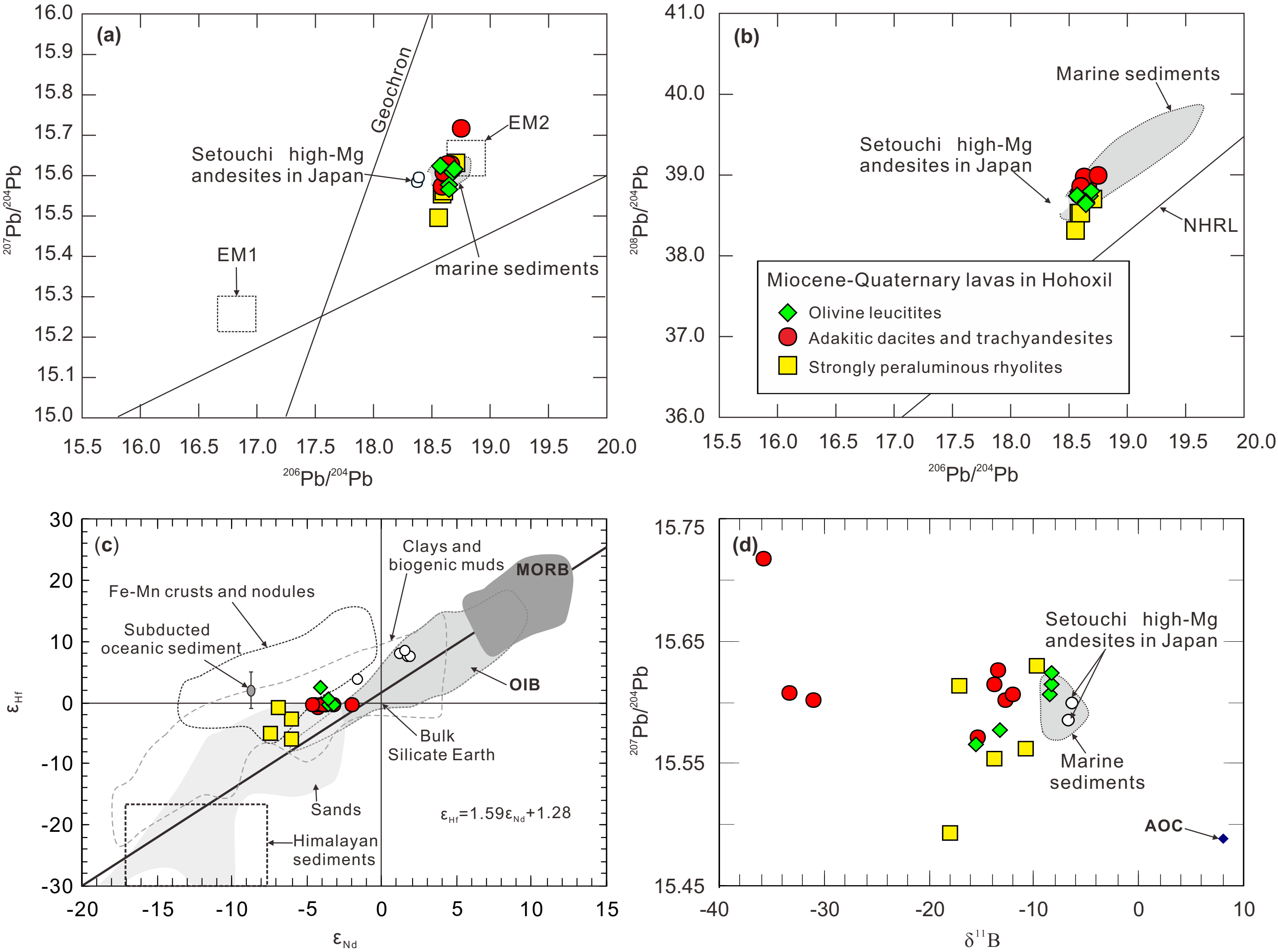
(a)
Geochron
EM2
Setouchi high-Mg andesites in Japan
EM1
marine sediments
$^{207}Pb/^{204}Pb$
$^{206}Pb/^{204}Pb$
(b)
Marine sediments
Setouchi high-Mg andesites in Japan
NHRL
$^{208}Pb/^{204}Pb$
$^{206}Pb/^{204}Pb$
Miocene-Quaternary lavas in Hohoxil
Olivine leucitites
Adakitic dacites and trachyandesites
Strongly peraluminous rhyolites
(c)
Clays and biogenic muds
MORB
Fe-Mn crusts and nodules
Subducted oceanic sediment
OIB
Bulk Silicate Earth
Sands
$\varepsilon_{Hf}=1.59\varepsilon_{Nd}+1.28$
Himalayan sediments
ε_{Hf}
ε_{Nd}
(d)
Setouchi high-Mg andesites in Japan
Marine sediments
AOC
$^{207}Pb/^{204}Pb$
$\delta^{11}B$

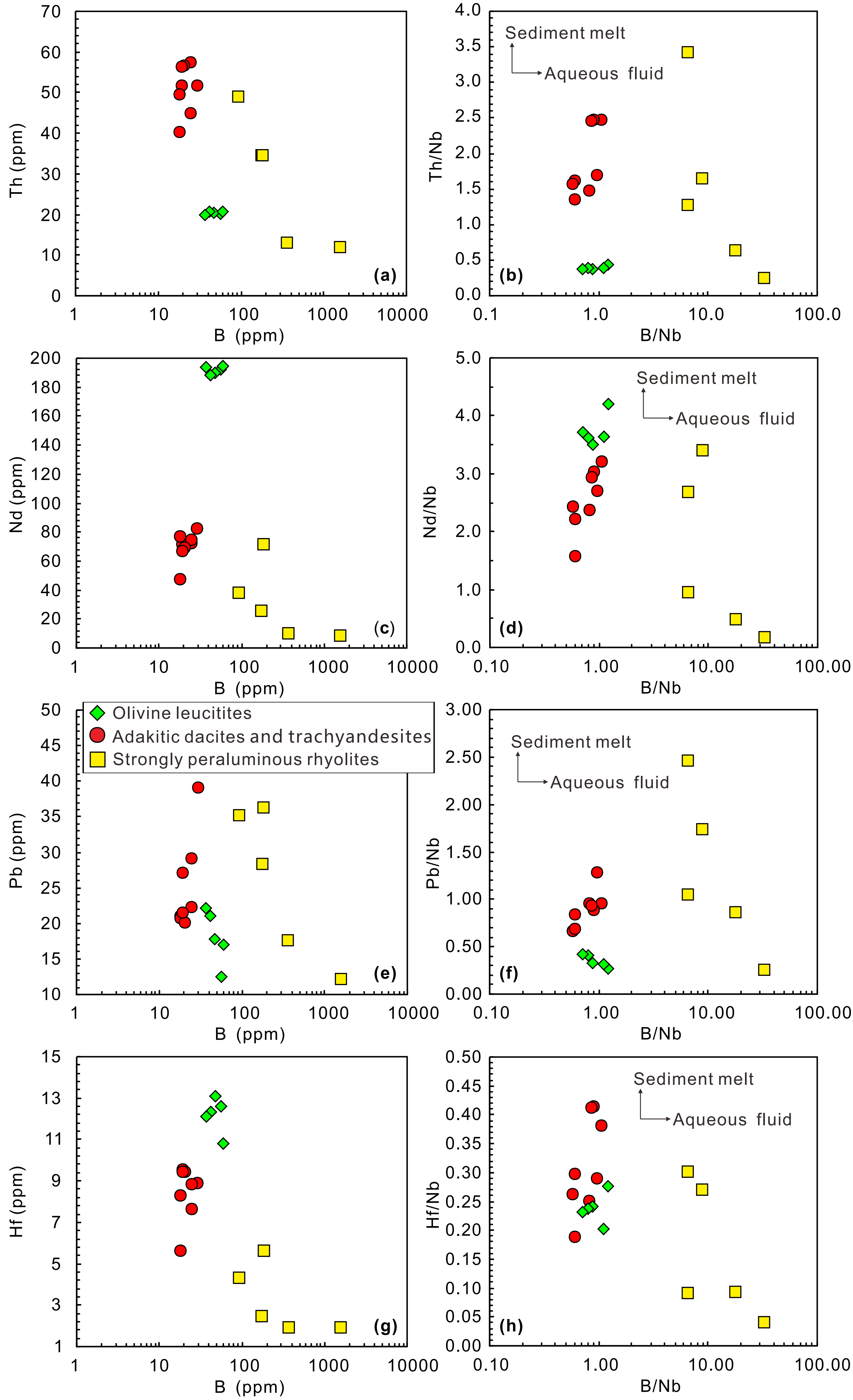

Th (ppm)
B (ppm)
(a)
Th/Nb
B/Nb
Sediment melt
Aqueous fluid
(b)
Nd (ppm)
(c)
Nd/Nb
(d)
Olivine leucitites
Adakitic dacites and trachyandesites
Strongly peraluminous rhyolites
Pb (ppm)
(e)
Pb/Nb
(f)
Hf (ppm)
(g)
Hf/Nb
(h)

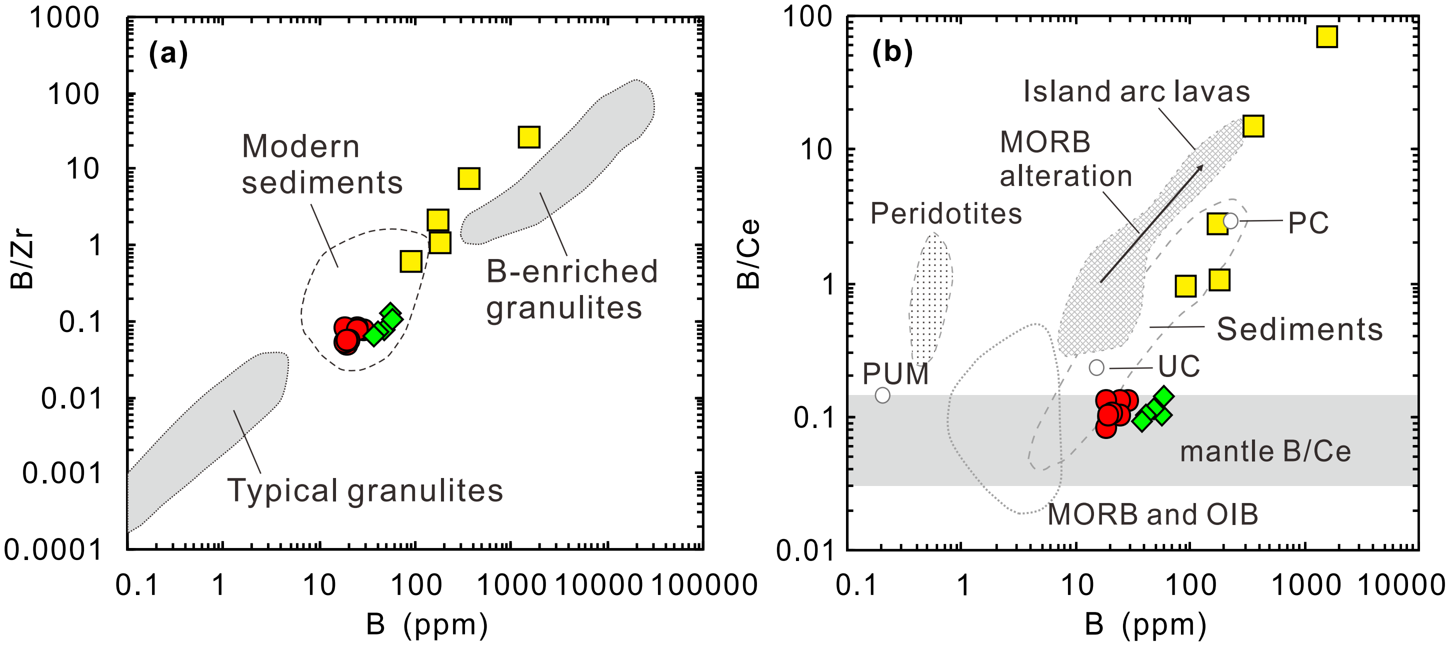

(a)
B/Zr
B (ppm)
Modern sediments
B-enriched granulites
Typical granulites
(b)
B/Ce
B (ppm)
Island arc lavas
MORB alteration
Peridotites
PC
Sediments
UC
PUM
mantle B/Ce
MORB and OIB

Supplementary data for

Sediment recycling by continental subduction indicated by B-Hf-Pb-Nd isotopes from Miocene–Quaternary lavas in the northern margin of Tibet

Xiu-Zheng Zhang [a, b], Qiang Wang[a, b, c*], Andrew C. Kerr[d], Gang-Jian Wei[a, b], Yue Qi[a], Ying Liu[a], Yu-Cheng Yang[a]

[a] *State Key Laboratory of Isotope Geochemistry, Guangzhou Institute of Geochemistry, Chinese Academy of Sciences, Guangzhou 510640, China*

[b] *CAS Center for Excellence in Deep Earth Science, Guangzhou, 510640, China*

[c] *College of Earth and Planetary Sciences, University of Chinese Academy of Sciences, Beijing 100049, China*

[d] *School of Earth and Environmental Sciences, Cardiff University, Cardiff CF10 3AT, UK*

Corresponding Author: * Qiang Wang, E-mail: wqiang@gig.ac.cn

Includes the following Materials

- Text S1 Methods
- Table S1 Boron (B) concentrations and isotopes for the Miocene–Quaternary lavas in the Hohxil area, northern Tibet
- Table S2 Hf-Pb-Nd isotopes for the Miocene–Quaternary lavas in the Hohxil area, northern Tibet

Text S1. Methods

1. Whole-rock Pb-Hf isotopic compositions

Whole-rock Pb-Hf isotope analyses were performed at the State Key Laboratory of Isotope Geochemistry, Guangzhou Institute of Geochemistry, Chinese Academy of Sciences (SKLaBIG, GIGCAS), Guangzhou, China. The powder samples were weighed into the Teflon beaker, spiked and dissolved in concentrated HF and 1:1 HNO3 at 180 °C for 7 days. Lead was separated and purified by conventional cation exchange technique (AG1× 8, 200-400 resin) with diluted HBr as an eluant. Total procedural blanks were less than 50 pg Pb. The measured lead isotopic ratios were normalized to $^{205}Tl/^{203}Tl$ = 2.38714. Repeated analyses of SRM981 yielded average values of $^{206}Pb/^{204}Pb$ = 16.9298± 4 (1SD), $^{207}Pb/^{204}Pb$ = 15.4821± 5 (1SD) and $^{208}Pb/^{204}Pb$ = 36.6718± 11 (1SD). The analyses of BHVO-2 standard yielded $^{206}Pb/^{204}Pb$, $^{207}Pb/^{204}Pb$, and $^{208}Pb/^{204}Pb$ ratios of 18.6287± 40, 15.5335± 25, and 38.2412± 55, respectively (1SD, n = 6), which were within errors of published values (e.g., Weis et al., 2006). About 100 mg of sample powder was mixed with 200 mg of $Li_2B_4O_7$, placed in a platinum crucible, and melted in a Rigaku high-frequency fusion apparatus at 1200 °C. The melt was cooled rapidly to form glasses that were dissolved in 2 M HCl. Hf was separated from the matrix and interfering elements by HCl-single-column Ln-Spec extraction chromatography. The Hf isotopic compositions of the selected samples were determined using a Micromass Isoprobe multicollector–inductively coupled plasma–mass spectrometry (MC–ICP–MS) system. The detailed analytical procedures are described in Li et al. (2006). The measured $^{176}Hf/^{177}Hf$ ratios were normalized to $^{176}Hf/^{177}Hf$ = 0.7325, and the measured $^{176}Hf/^{177}Hf$ ratio of the BHVO-2 standard, determined during analysis of the unknowns, was 0.283079 ± 0.000004 (2σ; n = 2).

2. Boron isotopic compositions

B abundance and B isotopic analyses were conducted in the SKLaBIG GIG-CAS. About 150 mg of rock powder was precisely weighed into a pre-cleaned 7 mL PFA-Teflon beaker, along with 100 µL 1% mannitol, 100 µL H_2O_2 and 3 mL 24 M HF. The beaker was tightly capped and placed on a hot plate at a temperature of 60°C for 30 days for boron extraction. Both the solution and residue were then transferred into a pre-cleaned polypropylene (PP) tube, and centrifuged. The supernatant was collected, and boron was concentrated in this solution, at a recovery of > 99% (Wei et al., 2013).

The collected supernatant was then diluted with B-free Milli-Q deionized water to an HF molarity of 3 M for ion-exchange purification. The samples were loaded onto 20 ml columns with Bio-Rad AG MP-1 strong anion exchange resin for chromatographic purification, following procedures in Wei et al (2013).

Boron concentration was determined using a Varian Vista Pro inductively coupled plasma atomic emission spectrometer (ICP-AES) equipped with an HF-resistant Teflon spray chamber and an Al_2O_3 injector. Boron was measured using the 249.678 nm spectral line. Internal precision for our boron concentration determinations were generally better than 5% (RSD). Basalt standards JB-2 and JB-3 were measured multiple times as unknowns with our samples, yielding B concentrations 29.98 ± 0.98 μg/g (1SD, n=6) and 19.39 ± 0.52 μg/g (1SD, n=6), respectively. Our results for B5 are consistent with the long-time monitoring value of 10.18 μg/g B in our laboratory. $\delta^{11}B$ measurements were performed using a Finnegan Neptune MC-ICPMS in sample standard-bracketing (SSB) mode. Details of the analytical procedures of $\delta^{11}B$ are described by Wei et al. (2013). The internal precision for $\delta^{11}B$ was better than ±0.05‰ (2s standard error), and the external precision for $\delta^{11}B$ was better than ±0.30‰ (2s standard error) estimated by the long-term results of SRM 951 (Wei et al., 2013). Several basalt standards such as JB-2 and JB-3 were repeatedly analyzed along with the samples, yielding the 7.03 ± 0.12 ‰ (1SD, n=6) and 5.94 ± 0.40 ‰ (1SD, n=6).

Table S1 **Boron (B) concentrations and isotopes for the Miocene–Quaternary lavas in the Hohxil area, northern Tibet**

Sample ID	B (ppm)	$\delta^{11}B$ (per mil)	B (ppm)	1SE	Location
Olivine leucitites (16 Ma)					
6304-1	41.7	−13.2	41.7	0.03	35°24’29"N; 91°15’48"E
6304B	55.9	−8.6	55.9	0.03	35°24’29"N; 91°15’48"E
6304C	47.3	−8.3	47.3	0.03	35°24’29"N; 91°15’48"E
6304E	59.3	−8.4	59.3	0.03	35°24’29"N; 91°15’55"E
6305	37.2	−15.6	37.2	0.04	35°24’02"N; 91°16’18"E
Strongly peraluminous rhyolites (9.0–1.5 Ma)					
2509	175	−13.7	175	0.03	35°58’09"N; 90°48’06"E
2511-1	184	−10.9	184	0.04	35°57’57"N; 90°47’15"E
1P2JD7-1	1559	−9.7	1559	0.04	35°47’26"N; 90°25’39"E
2011	364	−17.9	364	0.04	35°50’54"N; 90°29’4"E
2303	92.7	−17.0	92.7	0.04	35°45’12"N; 90°39’47"E
Adakitic dacites and trachyandesites (18–15 Ma)					
3P1 1-1	24.8	−13.5	24.8	0.03	35.876°N; 91.299°E
3P1 2-1	18.3	−13.7	18.3	0.03	
3302	19.4	−15.4	19.4	0.03	
3304-1	24.5	−31.1	24.5	0.03	
3302-1	29.2	−12.7	29.2	0.03	
3303	18.1	−12.0	18.1	0.03	
3304-3A	20.5	−35.7	20.5	0.04	
3304-3B	19.5	−33.3	19.5	0.04	

Note: 1SE for the internal error of $\delta^{11}B$.

Table S2 Hf-Pb-Nd isotopes for the Miocene–Quaternary lavas in the Hohxil area, northern Tibet

	Olivine leucitites (16 Ma)					Adakitic dacites and trachyandesites (18–15 Ma)							
Sample ID	**6304-1**	**6304B**	**6304C**	**6304E**	**6305**	**3P1-1**	**3P2-1**	**3302**	**3304-1**	**3302-1**	**3303**	**3304-3A**	**3304-3B**
T (Ma)	16	16		16	16	18	18	18	18	18	18	18	18
Lu	0.37	0.373		0.384	0.372	0.19	0.15	0.17	0.13	0.21	0.18	0.13	0.13
Hf	12.1	12.6		12.3	13	7.64	5.64	9.56	8.83	8.87	8.31	9.46	9.45
$^{176}Lu/^{177}Hf$	0.004332	0.004194		0.004423	0.004054	0.003523	0.003768	0.002519	0.002086	0.003354	0.003068	0.001947	0.001949
$^{176}Hf/^{177}Hf$	0.282770	0.282772		0.282783	0.282793	0.282752	0.282752	0.282752	0.282763	0.282752	0.282760	0.282766	0.282764
2SE	0.000026	0.000021		0.000015	0.000013	0.000009	0.000005	0.000003	0.000005	0.000003	0.000007	0.000005	0.000008
ε_{Hf} (0)	−0.08	0.01		0.39	0.76	−0.71	−0.71	−0.70	−0.32	−0.70	−0.44	−0.21	−0.27
ε_{Hf} (t)	0.23	0.33		0.70	1.08	−0.36	−0.36	−0.33	0.05	−0.34	−0.08	0.16	0.10
TDM(Ma)	750	743		731	707	760	765	738	714	755	738	706	709
	This study					**This study**							
$^{206}Pb/^{204}Pb$	18.638	18.681	18.689	18.568	18.639	18.656	18.627	18.579	18.609	18.611	18.625	18.751	18.605
$^{207}Pb/^{204}Pb$	15.577	15.607	15.615	15.624	15.565	15.626	15.615	15.571	15.602	15.602	15.606	15.717	15.608
$^{208}Pb/^{204}Pb$	38.672	38.734	38.809	38.749	38.644	38.864	38.845	38.757	38.808	38.812	38.885	39.005	38.867
	This study					**This study**							
Sm	27.95	28.41	28.25	27.82	28.89	9.038	6.085	9.018	8.977	10.11	9.589	8.476	8.059
Nd	188.6	191.9	189.7	194.9	194.1	72.13	47.23	71.49	74.68	82.76	77.11	69.42	67.15
$^{147}Sm/^{144}Nd$	0.090100	0.090100	0.090600	0.086829	0.090500	0.076200	0.078400	0.076700	0.073100	0.074300	0.075600	0.074300	0.073000
$^{143}Nd/^{144}Nd$	0.512469	0.512454	0.512427	0.512459	0.512453	0.512443	0.512444	0.512418	0.512531	0.512413	0.512431	0.512470	0.512403
2SE	0.000010	0.000008	0.000008	0.000012	0.000009	0.000010	0.000010	0.000016	0.000011	0.000024	0.000010	0.000010	0.000014
ε_{Nd} (0)	−3.30	−3.59	−4.12	−3.48	−3.61	−3.80	−3.78	−4.29	−2.09	−4.39	−4.04	−3.28	−4.58
ε_{Nd} (t)	−3.07	−3.37	−3.89	−3.25	−3.39	−3.53	−3.51	−4.02	−1.80	−4.11	−3.76	−3.00	−4.30
TDM(Ma)	840	859	895	830	863	784	796	815	672	806	794	744	810
	Qi et al., 2020					**Wang et al., 2005**							

	Strongly peraluminous rhyolites (9.0–1.5 Ma)				
Sample ID	**2509**	**2511-1**	**1P2JD7-1**	**2011**	**2303**
T(Ma)		2	3	9	9
Lu		0.089	0.046	0.058	0.087
Hf		5.64	1.93	1.92	4.32
^{176}Lu/^{177}Hf		0.002235	0.003376	0.004279	0.002853
^{176}Hf/^{177}Hf		0.282672	0.282625	0.282690	0.282750
2SE		0.000006	0.000002	0.000019	0.000007
ε_{Hf} (0)		−3.52	−5.20	−2.89	−0.79
ε_{Hf} (t)		−3.49	−5.14	−2.72	−0.61
TDM(Ma)		849	947	872	749
	This study				
^{206}Pb/^{204}Pb	18.587	18.603	18.701	18.562	18.636
^{207}Pb/^{204}Pb	15.554	15.562	15.63	15.493	15.613
^{208}Pb/^{204}Pb	38.533	38.522	38.699	38.309	38.742
	Wang et al., 2012				
Sm	4.65	11.6	1.66	2.08	6.32
Nd	25.4	71.2	8.32	9.87	38.3
^{147}Sm/^{144}Nd	0.111116	0.099135	0.121685	0.128318	0.100336
^{143}Nd/^{144}Nd	0.512329	0.512338	0.512256	0.512330	0.512279
2SE	0.000007	0.000011	0.000012	0.000012	0.000007
ε_{Nd} (0)	−6.03	−5.85	−7.44	−6.01	−7.00
ε_{Nd} (t)	−6.02	−5.83	−7.41	−5.93	−6.88
TDM(Ma)	1219	1080	1478	1462	1170
	Wang et al., 2012				

Reference

Li, X.H., Li, Z.X., Wingate, M.T.D., Chung, S.L., Liu, Y., Lin, G.C., Li, W.X., 2006. Geochemistry of the 755 Ma Mundine Well dyke swarm, northwestern Australia: Part of a Neoproterozoic mantle superplume beneath Rodinia? Precambr. Res. 146 (1–2), 1–15

Qi, Y., Wang, Q., Zhu, Y.T., Shi, L.C., Yang, Y.N., 2020. Miocene olivine leucitites in the Hoh Xil basin, northern Tibet: implications for intracontinental lithosphere melting and surface uplift of the Tibetan Plateau. J. Petrol. 61, 1–18

Wang, Q., Chung, S.L., Li, X.H., Wyman, D., Li, Z.X., Sun, W.D., Qiu, H.N., Liu, Y.S., Zhu, Y.T., 2012. Crustal Melting and Flow beneath Northern Tibet: Evidence from Mid-Miocene to Quaternary Strongly Peraluminous Rhyolites in the Southern Kunlun Range. Journal of Petrology 53(12), 2523–2566.

Wang, Q., Wyman, D.A., Xu, J., Dong, Y., Vasconcelos, P.M., Pearson, N., Wan, Y., Dong, H., Li, C., Yu, Y., Zhu, T., Feng, X., Zhang, Q., Zi, F., Chu, Z., 2008. Eocene melting of subducting continental crust and early uplifting of central Tibet: Evidence from central–western Qiangtang high-K calc-alkaline andesites, dacites and rhyolites. Earth and Planetary Science Letters 272, 158–171.

Wei, G. J., Wei, J. X., Liu, Y., Ke, T., Ren, Z. Y., Ma, J. L., and Xu, Y. G., 2013, Measurement on high-precision boron isotope of silicate materials by a single column purification method and MC-ICP-MS: Journal of Analytical Atomic Spectrometry, v. 28, no. 4, p. 606-612.

Weis et al., 2006. High-precision isotopic characterization of USGS reference materials by TIMS and MC-ICP-MS. Geochemistry, Geophysics, Geosystems, 7, Q08006.